A quantum cascade laser-pumped molecular laser tunable over 1 THz

ARMAN AMIRZHAN[1,†], PAUL CHEVALIER[1,†], JEREMY ROWLETTE[2], H. TED STINSON[2], MICHAEL PUSHKARSKY[2], TIMOTHY DAY[2], HENRY O. EVERITT[3,4,*], AND FEDERICO CAPASSO[1,*]

[1] *Harvard John A. Paulson School of Engineering and Applied Sciences, Harvard University, Cambridge, MA, 02138*
[2] *DRS Daylight Solutions, San Diego, CA 92128*
[3] *U.S. Army Combat Capabilities Development Command Aviation and Missile Center, Redstone Arsenal, AL 35898*
[4] *Department of Physics, Duke University, Durham, NC 27708*
[*] *Corresponding authors: capasso@seas.harvard.edu, everitt@phy.duke.edu*
[†] *These authors contributed equally to this paper.*

Compiled May 28, 2021

By introducing methyl fluoride (CH_3F) as a new gain medium for a quantum cascade laser-pumped molecular laser (QPML), we demonstrate continuous-wave lasing from more than 120 discrete transitions spanning the frequency range 0.25 to 1.3 THz. The unprecedented degree of spectral tuning achieved with CH_3F also confirms the universality of the QPML concept: for all polar gas molecules, lasing can be induced on any dipole-allowed rotational transition by sufficient pumping of a related roto-vibrational transition using a continuously tunable quantum cascade laser.

http://dx.doi.org/10.1364/ao.XX.XXXXXX

As field of terahertz (THz) technology rapidly grows, with exciting applications in radio astronomy [1], biomedicine [2], defense and security, communication, aerospace [3], and other fields, the generation and detection of THz radiation remains a challenge. Despite decades of extensive research in the area, few practical sources of THz radiation exist. Vacuum electronic devices and multiplier chain sources struggle to reach frequencies above 1 THz, free electron lasers and optically pumped far infrared lasers (OPFIR) are bulky in size, and difference frequency photomixers produce broad linewidths and low output power [4]. THz quantum cascade lasers, despite recent advances, can operate only in pulsed mode using thermoelectric coolers [5] and require cryogenic cooling for cw operation [6].

A new source of powerful, widely tunable THz radiation has been recently demonstrated: the Quantum Cascade Laser (QCL) pumped molecular laser (QPML) [7–9]. The QPML is an OPFIR laser [10, 11], but with a compact, continuously tunable mid-infrared (IR) QCL used as a pumping source instead of a bulky, line tunable mid-infrared gas laser. The continuous tunability of QCLs allows pumping of any roto-vibrational transition for gas phase molecules with a permanent electric dipole moment. Pumping these roto-vibrational transitions, which typically lie in the mid-infrared spectral range, creates population inversions in dipole-allowed transitions between adjacent rotational energy levels, with frequencies typically in the THz range. Placing this molecular gain medium in a small laser cavity [11, 12] creates a room temperature cw laser in a compact form factor with the potential for wide frequency tunability throughout the THz region.

We have previously demonstrated the QPML concept by using an external cavity QCL as a pump source and nitrous oxide as a molecular gain medium, achieving continuous-wave laser emission for 39 transitions with discrete line tunability from 250 GHz up to 1 THz [8]. The first demonstration of a QPML used ammonia gas molecules (NH_3) as a gain medium [7] and was based on population inversion of pure inversion transitions in the $\nu_2 = 1$ excited vibration band. Such pure inversion transitions can achieve high output power, with more than 1 mW demonstrated recently [13]), but with a tuning range limited to frequencies around 0.9 to 1.1 THz. Another QPML demonstration using ammonia [9] created five lasing lines in the range from 4.4 to 4.5 THz using direct rotational transitions in the same $\nu_2 = 1$ excited vibration band.

Here, we demonstrate a new QPML by introducing and exploring methyl fluoride (CH_3F) as the gas-phase molecular gain medium. The Q and R branches of many roto-vibrational transitions from levels between $J = 5$ to 25 were pumped with an external cavity QCL, and laser emission was obtained for more than 120 lines spanning more than 1 THz over the frequency range 0.25 - 1.3 THz. These demonstrations confirm the universality of the QPML concept: population inversions and lasing can be achieved on almost any dipole-allowed rotational transition in virtually any polar gas molecule when an associated roto-vibrational transition is sufficiently pumped by a QCL.

In our first reported QPML laser, we used the linear polar molecule nitrous oxide (N_2O), which has a simple roto-vibrational spectrum with only one quantum number (J) defining rotational energy levels. By contrast, methyl fluoride is a prolate symmetric top molecule (see Fig. 1A inset) whose more complex roto-vibrational energy level structure is characterized by two quantum numbers: J, representing the total angular momentum, and K, representing the projection of the angular momentum along the main symmetry axis.

The energies of the rotational states within a given vibrational energy band, up to the 4-th order in J and K [14], are given by

$$F(J,K) = BJ(J+1) + (A-B)K^2 - D_J J^2(J+1)^2 - D_{JK}J(J+1)K^2 - D_K K^4, \quad (1)$$

where B and A are rotational constants, and D_J, D_{JK}, and D_K are centrifugal distortion constants, unique for each vibrational energy band. A more thorough polynomial development given in the supplementary information (SI). As methyl fluoride is a prolate symmetric top molecule, its rotational constant A ($\approx$ 150 GHz) is larger than B ($\approx$ 25 GHz) [15], so the energy of rotational states increases with increasing J and K. The laser transition frequency between adjacent rotational energy states can be calculated using equation 1 to be:

$$\nu(J,K) = F(J+1,K) - F(J,K) = 2B(J+1) - 4D_J(J+1)^3 - 2D_{JK}(J+1)K^2 \quad (2)$$

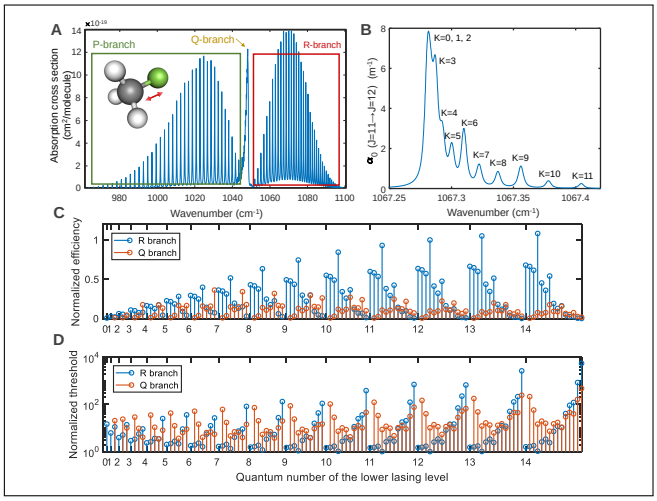

Fig. 1. (A) Room temperature IR spectrum of the $\nu_3 = 1$ roto-vibrational band of CH_3F around 1000 cm^{-1}, showing the absorption cross sections as a function of wavenumber for the P, Q, and R branch transitions, using data obtained from the HITRAN database[16, 17]. (B) Simulated room temperature spectrum of the Doppler broadened R-branch roto-vibrational transitions from the $J_L = 11$ ground vibrational level at 30 mTorr, using [15]. Calculated power efficiency (C) and threshold (D) plotted as a function of lower laser level J and K, normalized by the respective values for the $J = 13 \rightarrow 12$, $K = 3$ transition.

Our QCL frequency could be tuned across the lowest energy ν_3 vibrational band of CH_3F [18], whose IR spectrum is shown in Fig. 1(A) and whose carbon-fluorine stretching is illustrated in inset. This molecular gain medium is pumped from a ground state rotational level with quantum numbers J_L, K_L to a rotational state in the $\nu_3 = 1$ vibrational level with quantum numbers J_U, K_U. The dipolar selection rules of this particular band prohibit a change in K quantum number, while ΔJ = 0, -1 or 1 [14]. The CH_3F gain medium was pumped either with an R-branch transition ($J_U = J_L + 1$, $K = K_U = K_L$) or a Q- branch transition ($J_U = J_L$, $K = K_U = K_L \neq 0$). P-branch infrared transitions could have been pumped too, but they are so similar to R-branch transitions, except for their frequency, that they were not considered here. A given $J_L \rightarrow J_U$ infrared transition exhibits an increasing number of lines with increasing J_L whose frequencies separate quadratically with K because of centrifugal distortion, as can be seen in Fig. 1(B).

For an R-branch pump, a population inversion can occur within the $\nu_3 = 1$ vibrational state between levels with quantum numbers $J_L + 1$ and J_L, while pumping a Q-branch transition originating from the same J_L level leads to inversion between levels with quantum numbers J_L and $J_L - 1$. Because the emission frequency from equation 2 depends on K, for a given J_U there are J_U possible laser transitions ($K = 0$ to $J_U - 1$) for P- or R-branch pumping and $J_U - 1$ possible laser transitions ($K = 1$ to $J_U - 1$) for Q-branch pumping. It is this increasing number of discrete laser lines with increasing J_U that makes CH_3F an attractive gain medium for high tunability, achieved by selectively pumping roto-vibrational transitions of different K values.

The THz emission power and lasing threshold of the CH_3F QPML, which can be estimated using a comprehensive model [12] that considers all molecular relaxation mechanisms, can be reasonably approximated by a far simpler model [8] in the low pressure regime where the rate of unfavorable molecular dipole-dipole collisions is smaller than the rate of favorable hard collisions with the cavity walls. The salient expressions, recalled in the SI, indicate that at a given frequency the output power increases and the lasing threshold decreases with increasing absorption strength of the pumped infrared transition.

Although actual laser power and threshold sensitively depend on cavity geometry and loss, the simple model thereby indicates that one may ascertain the relative efficacy of the allowed laser transitions when pumped by P, Q, or R-branch transitions by comparing their relative IR absorption strengths. These can be easily calculated (see SI) using equation 1 and the known degeneracies to estimate the fractional occupation of J_L, K_L, multiplied by the branching ratio for the considered IR pumping branch (P, Q, or R). The relative power efficiency is calculated by multiplying the relative IR absorption by J_U to account for the frequency dependence of the laser transition, and the relative lasing threshold is calculated by multiplying the relative IR absorption by the branching ratio for the lasing transition. For CH_3F QPML lines, these are normalized to the transition with lowest threshold ($J = 13 \rightarrow 12$, $K = 3$) and compared in Figs. 1(C) and 1(D), respectively as a function of the lower lasing level quantum numbers. Notice that the lowest thresholds generally occur for low K lines when pumped by R (and P) branch transitions but for mid-range K lines when pumped by Q branch transitions. Likewise, the highest power efficiencies generally occur for $K = 3$ lines when pumped by R (or P) branch transitions and $K = 6$ lines for Q branch pumping.

Figure 2 shows the experimental setup. The IR pump is provided by an external cavity (EC)-QCL (Daylight Solutions 41095-HHG-UT, tunable from 920 to 1194 cm^{-1}). The THz cavity is a copper pipe with a 4.8 mm internal diameter and 50 cm in length. A flat mirror with a centered 1 mm diameter pinhole was used as the output coupler. The cavity resonance frequency was tuned by changing the tuning mirror position to adjust the cavity length. A separate CH_3F gas absorption cell was used so that the QCL emission frequency could be precisely tuned to a desired CH_3F roto-vibrational transition.

The QCL pump beam was coupled into the THz laser cavity through the pinhole in the output coupler using an anti-reflective coated ZnSe lens to focus the beam into the pinhole. A 2 mm thick ZnSe window mounted at the Brewster angle was used to maximize the amount of QCL power injected into the vacuum-

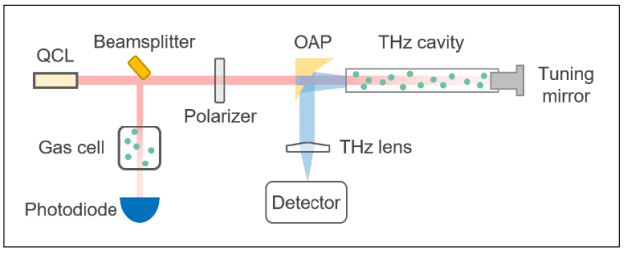

Fig. 2. Schematic of the experimental setup. A gold-plated silicon wafer was used as a beamsplitter to reflect a small portion of the pump beam into the reference gas cell, while the rest entered the THz cavity. The following detectors were used to detect lasing lines: Schottky diodes between 0.25 and 1.1 THz, a Golay cell above 1.1 THz, and heterodyne receivers to measure spectra between 0.3 and 1.1 THz.

tight gas laser cavity. A wire grid polarizer mounted on a rotational stage was used as a variable attenuator for the linearly polarized QCL beam. The injected IR power was measured by replacing the tuning mirror with a ZnSe window and measuring the pump beam power transmitted through the THz cavity.

The off-axis parabolic mirror (OAP) used to collect the generated THz laser radiation had a hole drilled along the focal axis through which the pump beam was coupled into the THz laser cavity. A polytetrafluoroethylene (PTFE) lens blocked any residual IR signal and focused the collected THz beam onto the Schottky diode detector, the Golay cell, or the heterodyne receiver. The THz output power was measured using a calibrated calorimeter-style power meter.

The theoretically predicted output power of a CH_3F QPML pumped by a 150 mW QCL with a gas pressure of 20 mTorr is plotted in Fig. 3(A). This plot was obtained using the simple model previously mentioned [8] assuming that the gain medium was pumped using an R-branch transition with $J_L = 1$ to 50, and $K = 3$ (except for J_L<3 where $K = 0$ was assumed). Maximum QPML power is expected between 0.8 to 1.3 THz.

Laser emission was obtained experimentally by tuning the QCL into coincidence with a roto-vibrational transition of the gain medium and then by tuning the cavity resonance into coincidence with the lasing rotational transition by adjusting the cavity length. Emission was achieved from 0.25 THz to 1.3 THz by pumping roto-vibrational transitions of CH_3F originating from a level with quantum number J_L spanning from 5 to 25, and various K numbers. Of the 315 possible lasing lines over this range, emission was observed for at least 120 of them, including many measured using a heterodyne receiver that are plotted together in Fig. 3(B). In Fig. 3(C), a detailed view of lasing lines obtained around 604 GHz is shown, indicating which lines were pumped by an R-branch transition or a Q-branch transition. As anticipated, lines with larger K quantum number were more efficiently pumped with Q-branch transitions, while the lines with lower K quantum number were more efficiently pumped with R-branch transitions. Because the lower K lines are spectrally close together, we were routinely able to induce two, three, even four transitions to lase simultaneously with R-branch pumping.

The output power of the THz laser emission depends on a combination of many parameters, including the infrared pumping efficiency, the choice of the gain medium, and the laser cavity design and geometry [19]. The pumping efficiency will be primarily affected by the available QCL power and the overlap between the QCL emission linewidth and the gain medium absorption bandwidth. The choice of the gain medium will be motivated by many properties, including its IR absorption coefficient and saturation, the dipole moments of the lasing transitions, the dipole-dipole collision rate, and the ratio of the emission frequency to the pump frequency. The effects of the laser cavity are determined by its geometry, cavity quality factor, loss factor of pump power inside the cavity, and the THz losses in the output coupler. All the above factors must be considered in calculating the optimum THz cavity length, diameter, output coupling ratio, and gas pressure. Increasing the cavity diameter results in improved cavity Q factor and reduced pump saturation, but at the expense of increased inversion quenching caused by the reduced relaxation rate through wall collisions. Optimal cavity dimensions, operating pressure, and more accurate output powers are calculated by performing extensive molecular dynamics simulations [12, 19].

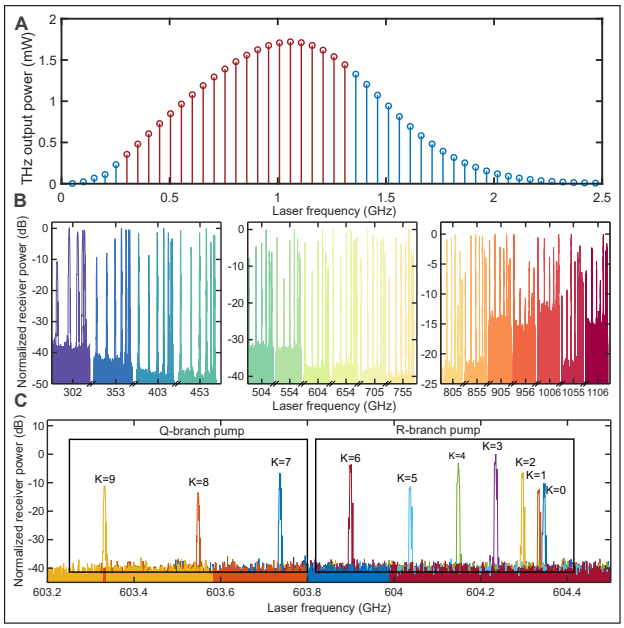

Fig. 3. (A) Plot of the THz emission power, approximated using a simple model of a 20 mTorr CH_3F QPML pumped with a 150 mW QCL, as a function of the frequency for a 4.8 mm diameter, 50 cm long cell. Red lines represent transitions at which laser emission was achieved. (B) Experimental data showing all lines measured using a heterodyne receiver, from 302 GHz to 1106 GHz. (C) Detailed view of measured lasing lines emitting around 603 GHz showing which lines were pumped with an R or a Q branch transition.

The laser performance has been measured experimentally at various gas pressures and pump powers. The experiment was conducted by setting the pressure to a fixed value, then slowly adjusting the QCL pump power while measuring the THz signal strength using a Schottky diode detector. By referencing the measured signal strength against the largest measured power for a given lasing transition, a surface plot of normalized THz output signal as a function of pump power and pressure could be constructed, such as shown in Fig. 4(A) for the $J = 12 \rightarrow 11$, $K = 3$ lasing transition near 604 GHz and in Fig. 4(B) for the $J = 22 \rightarrow 21$, $K = 3$ lasing transition near 1.1 THz.

The total collected power was measured using a calibrated calorimeter-style power meter (VDI PM5B). The largest measured THz power (13 µW) was obtained for the $J = 12 \rightarrow 11$,

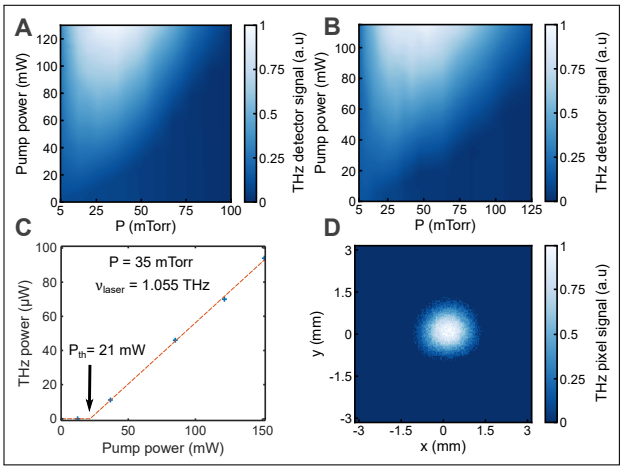

Fig. 4. Experimental data showing the detected THz signal as a function of gas pressure and infrared pump power at (A) 604 GHz and (B) 1.1 THz. (C) Output power vs. pump power curve obtained with a gas pressure of 35 mTorr at 1.055 THz. (D) Profile of the THz focused spot for the same transition measured with a microbolometer camera.

$K = 3$ transition near 604 GHz, for a pump power of 145 mW at a pressure of 30 mTorr. About 9.5 μW of collected power was measured at around 1.055 THz (for the $J = 21 \rightarrow 20$, $K = 3$ transition) for a pump power of 150 mW at a pressure of 35 mTorr. The collection efficiency of emitted power through the ZnSe Brewster window, the off-axis parabolic mirror, and the PTFE lens was experimentally estimated at most at 10%, which corresponds to a total emitted power of at least 130 μW at 604 GHz and at least 95 μW at 1.055 THz. The estimated emitted THz power as a function of pump power is plotted in Fig. 4(C), where the collected power was measured for five different pump power values (blue crosses); the red dashed line is a linear fit of the THz power above threshold. A clear threshold of around 21 mW pump power can be seen. The profile of the laser spot, as focused by the PTFE lens for the same transition, was measured using a microbolometer camera (INO Microxcam 384i-THz) and is shown in Fig. 4(D). The spot was fitted with a two-dimensional Gaussian model with spot sizes $2w_x = 2.08$ mm and $2w_y = 1.89$ mm.

As can be seen from the surface plots, the optimal pressure required to achieve the largest THz output power depends on the pump power as well as on the THz emission frequency. Away from this optimal pressure, the threshold pump power is increased and the THz output power is reduced with increasing pressure due to the increasing rate of dipole-dipole collisions or with decreasing pressure due to reduced population and pump saturation. The optimal pressure increases with increasing pump power to avoid the gain medium saturation. Comparing different laser transitions, the largest THz output power occurs when the highest population inversion is obtained, determined primarily by the absorption strength of the pumped transition and the Manley-Rowe effect. Consequently, the output power will vary significantly with THz emission frequency, as shown in Figure 3(A). Because the QPML grew increasingly sensitive to cavity misalignment with increasing frequency, more power was measured at 604 GHz than at 1.055 THz, a problem that will be overcome with improved cavity design.

We have shown how using a widely tunable external cavity quantum cascade laser to pump gaseous methyl fluoride, a prolate symmetric top molecule with a large dipole moment, created a widely tunable THz laser with many lasing lines. It is this wide tunability, coupled with prior demonstrations of low operating threshold, high operating frequency, and compact size, that make QPML's a leap-ahead source technology for generating THz radiation [7–9].

Funding. This work was partially supported by the U.S. Army Research Office (contracts W911NF-19-2-0168, W911NF-20-1-0157). Any opinions, findings, conclusions, or recommendations expressed in this material are those of the authors and do not necessarily reflect the views of the Assistant Secretary of Defense for Research.

Acknowledgments. The external cavity QCL used in the experiments was provided by DRS Daylight Solutions. The authors acknowledge Stanley Cotreau and Andrew DiMambro of Harvard University Instructional machine shop for their help with fabrication of the THz cavity elements.

Disclosures. The authors declare no conflicts of interest.

Data availability. Data underlying the results presented in this paper are not publicly available at this time but may be obtained from the authors upon reasonable request.

Supplemental document. See Supplement 1 for supporting content.

REFERENCES

1. A. Wootten and A. R. Thompson, Proc. IEEE **97**, 1463 (2009).
2. Q. Sun, Y. He, K. Liu, S. Fan, E. P. Parrott, and E. Pickwell-MacPherson, Quant. imaging medicine surgery **7**, 345 (2017).
3. F. Ellrich, M. Bauer, N. Schreiner, A. Keil, T. Pfeiffer, J. Klier, S. Weber, J. Jonuscheit, F. Friederich, and D. Molter, J. Infrared, Millimeter, Terahertz Waves **41**, 470 (2020).
4. E. Bründermann, H.-W. Hübers, and M. F. Kimmitt, "Sources," in *Terahertz Techniques*, (Springer, 2012), pp. 103–168.
5. A. Khalatpour, A. K. Paulsen, C. Deimert, Z. R. Wasilewski, and Q. Hu, Nat. Photonics **15**, 16 (2021).
6. M. Wienold, B. Röben, L. Schrottke, R. Sharma, A. Tahraoui, K. Biermann, and H. Grahn, Opt. Express **22**, 3334 (2014).
7. A. Pagies, G. Ducournau, and J.-F. Lampin, APL Photonics **1**, 031302 (2016).
8. P. Chevalier, A. Amirzhan, F. Wang, M. Piccardo, S. G. Johnson, F. Capasso, and H. O. Everitt, Science **366**, 856 (2019).
9. M. Wienold, A. Zubairova, and H.-W. Hübers, Opt. Express **28**, 23114 (2020).
10. T. Chang and T. Bridges, Opt. Commun. **1**, 423 (1970).
11. H. O. Everitt, D. D. Skatrud, and F. C. DeLucia, Appl. Phys. Lett. **49**, 995 (1986).
12. F. Wang, J. Lee, D. J. Phillips, S. G. Holliday, S.-L. Chua, J. Bravo-Abad, J. D. Joannopoulos, M. Soljačić, S. G. Johnson, and H. O. Everitt, Proc. Natl. Acad. Sci. **115**, 6614 (2018).
13. J.-F. Lampin, A. Pagies, G. Santarelli, J. Hesler, W. Hansel, R. Holzwarth, and S. Barbieri, Opt. Express **28**, 2091 (2020).
14. C. H. Townes and A. L. Schawlow, *Microwave spectroscopy* (Dover Publications, 1975).
15. D. J. Phillips, E. A. Tanner, F. C. De Lucia, and H. O. Everitt, Phys. Rev. A **85**, 052507 (2012).
16. R. Kochanov, I. Gordon, L. Rothman, K. Shine, S. Sharpe, T. Johnson, T. Wallington, J. Harrison, P. Bernath, M. Birk, G. Wagner, K. L. Bris, I. Bravo, and C. Hill, J. Quant. Spectrosc. Radiat. Transf. (2019).
17. S. W. Sharpe, T. J. Johnson, R. L. Sams, P. M. Chu, G. C. Rhoderick, and P. A. Johnson, Appl. Spectrosc. **58**, 1452 (2004).
18. A. Gambetta, E. Vicentini, Y. Wang, N. Coluccelli, E. Fasci, L. Gianfrani, A. Castrillo, V. Di Sarno, L. Santamaria, P. Maddaloni *et al.*, Opt. Lett. **42**, 1911 (2017).
19. F. Wang, S. G. Johnson, and H. O. Everitt, arXiv preprint arXiv:2101.11158 (2021).

A quantum cascade laser-pumped molecular laser tunable over 1 THz: supplemental document

This document contains additional details about the experimental work, the spectroscopy of methyl fluoride, and some additional theoretical predictions.

1. ENERGY LEVELS OF A SYMMETRIC TOP MOLECULE

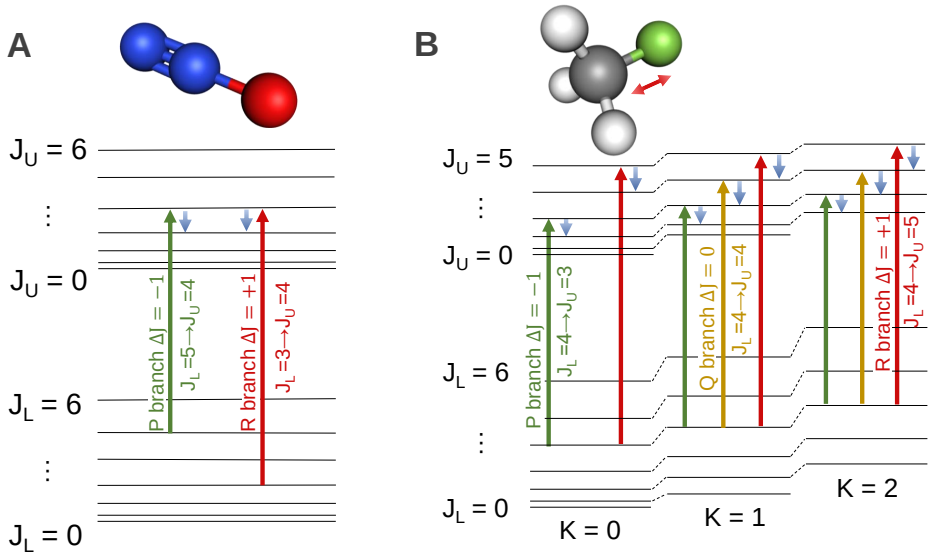

Fig. S1. (A) Diagram of the rotational energy levels in the ground (labeled J_L) and excited (labeled J_U) vibrational states of a linear molecule (e.g. N_2O). A three-dimensional schematic of the N_2O molecule is given in inset. (B) Diagram of the rotational energy levels in the ground state (J_L,K) and excited vibrational state (J_U,K) for a symmetric top molecule (e.g. CH_3F). A three-dimensional schematic of the CH_3 molecule is given in inset with a red arrow indicating the v_3 carbon-fluorine stretching vibrational mode considered in this paper. The green, yellow and red arrows represent respectively P, Q, and R branch infrared transitions, while the blue arrows represent the corresponding lasing transitions.

In our previously reported QPML laser, we used nitrous oxide (N_2O), a linear molecule with only one unique non-zero moment of inertia. Such a molecule has a simple roto-vibrational spectrum with only one quantum number (J) defining rotational energy levels (see Fig. S1(A)). Methyl fluoride (also known as fluoromethane or CH_3F), on the other hand, is a prolate symmetric top molecule (see Fig. S1B inset). Compared to the linear rotor, the symmetric top geometry has a more complex roto-vibrational energy level structure, with two quantum numbers defining the molecule's rotational energy levels, as shown in Fig. S1(B). The first quantum number, J, represents the total angular momentum, while the second quantum number K defines the projection of the angular momentum along the main symmetry axis. The selection rules prohibit a change in K quantum number, while the change in J number ΔJ must be 0, -1 or 1[1]. In Fig. S1(B), red arrows identify R-branch infrared transitions initiating from the same J_L quantum number but with different K quantum numbers (respectively green and yellow arrows for P and Q branch transitions). Q-branch transitions cannot occur between $K = 0$ levels for the v_3 vibrational mode (and all other symmetrical modes) of CH_3F. Each infrared transition corresponding to different K values will have a unique frequency, which can be seen as absorption peaks in Fig. 1(B) of the main text. Pumping each transition will create population inversion between rotational

energy levels, leading to stimulated emission with different emission frequencies, which are shown as blue arrows in Fig. S1(B). Therefore, it is possible to have finite discrete tunability of the THz emission frequency for a transition between two given J quantum numbers by selectively pumping roto-vibrational transitions of different K values.

The Equation 1 and 2 of the main text simply approximate the rotational energy levels of the CH_3F molecule. For the sake of simplicity we only introduced in the main text the development up to the 4-th order in powers of J and K. However the rotational constants for methyl fluoride have been experimentally fitted up to the 8-th order in power of J and K [2]. Sextic and hexic constants are required to properly calculate the vibrational transition energy for the molecules. The following equation is used to calculate energies of rotational states within a vibrational energy band up to the 8-th order in J and K[1, 2]:

$$\begin{aligned} F(J,K) =& BJ(J+1) + (A-B)K^2 \\ & - D_J J^2(J+1)^2 - D_{JK} J(J+1)K^2 - D_K K^4 \\ & + H_J J^3(J+1)^3 + H_{JJK} J^2(J+1)^2 K^2 + H_{JKK} J(J+1)K^4 + H_K K^6 \\ & + L_J J^4(J+1)^4 + L_{JJJK} J^3(J+1)^3 K^2 + L_{JJKK} J^2(J+1)^2 K^4 + L_{JKKK} J(J+1)K^6 + L_K K^8 \end{aligned} \tag{S1}$$

where J and K are rotational quantum numbers, B and A are rotational constants, D_J, D_{JK}, and D_K, H_J, H_{JJK}, H_{JKK}, H_K, L_J, L_{JJJK}, L_{JJKK},L_{JKKK} and L_K are centrifugal distortion constants. Rotational and centrifugal distortion constants are unique for each vibrational energy band. As methyl fluoride is a prolate symmetric top molecule its rotational constant A ($\approx$ 150 GHz) is always larger than B ($\approx$ 25 GHz) [2]. This results in increasing energy of rotational states with increasing K. The energy difference between adjacent rotational energy states defines the output THz lasing frequency and can be calculated using equation S2 up to the 8-th order in J and K. The dominant term for small values of K corresponds to a quadratic decrease of the lasing frequency with increasing K as can be seen further in Fig. 3(C) of the manuscript.

$$\begin{aligned} & F(J+1,K) - F(J,K) = 2B(J+1) - 4D_J(J+1)^3 - 2D_{JK}(J+1)K^2 \\ & + H_J(J+1)^3((J+2)^3 - J^3) + 4H_{JJK}(J+1)^3K^2 + 2H_{JKK}(J+1)K^4 \\ & + L_J(J+1)^4((J+2)^4 - J^4) + 6L_{JJJK}(J+1)^3((J+2)^3 - J^3)K^2 \\ & + 4L_{JJKK}(J+1)^3K^4 + 2L_{JKKK}(J+1)K^6 \end{aligned} \tag{S2}$$

2. DETAILS ON THE LASER OPERATION

The pressure in the laser cell is controlled similar to the way described in our previous work [3], recycling the gas by cryogenic pumping in order to minimize waste. First, the cell is evacuated to a very high vacuum ($P < 10^{-5}$ mTorr) by means of a rough rotary vane pump (Varian DS102) and a turbo molecular pump (Varian Turbo V81). Gas phase methyl fluoride is contained in a small 10 mL metallic cylinder connected to the system with a needle valve. This cylinder is cooled down by liquid nitrogen which causes the gas to solidify. After this initial cool down, the valve to the vacuum pump is closed and the valve of the cylinder is open. Then the liquid nitrogen is removed and the cylinder is let to warm, which causes the gas to sublime to fill the rest of the system. The valve of the cylinder is closed when the proper pressure (measured by a thermocouple Gauge (Alcatel) and an absolute manometer (MKS Bar-a-tron, range 1 Torr)) is achieved. To remove gas from the system, the cylinder is cooled again and the valve is opened until the gas is recovered and the laser system is empty.

In order to achieve laser emission, first the gas cell is filled with gas at the desired pressure, then the QCL is tuned to a desired gas absorption line by setting the correct drive current, grating position, and laser temperature in the QCL controller. The precised drive conditions of the QCL are achieved by monitoring the transmission of the QCL through a reference gas cell containing 50 mTorr of CH_3F. Finally laser emission at submillimeter wavelength is obtained by tuning the length of the cavity into resonance with the transition frequency.

3. SATURATION OF THE INFRARED PUMP

When the back mirror of the cavity is removed and replaced by a vacuum-tight, anti-reflection coated Zinc Selenide window, one can study how much light is absorbed by the gas as a function

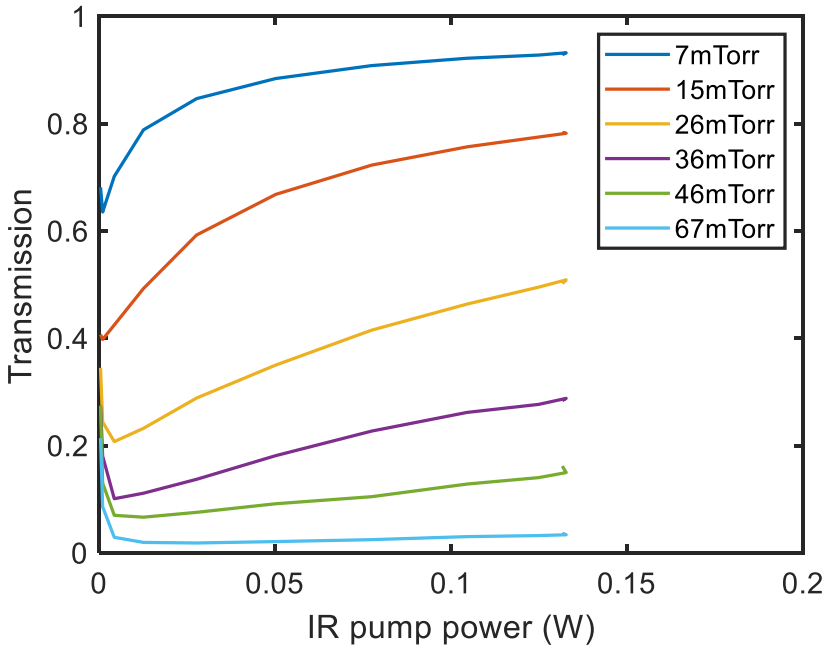

Fig. S2. Plot showing the transmission of the infrared pump through the laser cell as a function of the infrared power for different gas pressures. The infrared power is varied by means of a rotating polarizer. The QCL frequency was tuned to the $J = 11 \rightarrow J = 12, K = 3$ transition of the vibrational mode described in the manuscript.

of the infrared power during single pass through the cavity. The ratio of the transmitted power with gas in the cavity to the power transmitted without gas in the cavity is plotted as a function of the coupled infrared power in Fig S2 for different pressures of the gas. This plot shows the gas IR absorption strength strongly depends on the QCL input power, especially at low gas pressure. This indicates a strong saturation of the infrared absorption that is due to the narrow linewidth of the QCL relative to the bandwidth of the IR transition (the Doppler broadened full width half maximum at 1050 cm^{-1} is 67 MHz, the QCL linewidth is estimated around 1 MHz).

This strong pump saturation at low pressures may be the greatest bottleneck of our laser cavity for reaching higher output power. This limitation can be overcome by using a better optimized cavity geometry and different pumping conditions, something that will be an objective of future work.

4. THZ POWER VS PUMP DETUNING

The mid-infrared QCL can be continuously tuned around the peak absorption of the gas IR transition. Tuning of the QCL into the transition is typically achieved by tuning the laser temperature using small increments. Once laser emission is achieved, the QCL frequency can be continuously swept around the absorption line, and the THz signal can be monitored with the detector. Because the two counter propagating waves in the laser cavity encounter different gas velocity sub-classes, a Lamb dip-like feature is observed at the zero detuning point.

The measured THz signal at 604 GHz ($J = 12 \rightarrow 11, K = 3$ transition) is plotted in Fig. S3(A) as a function of the pump detuning. Figures S3(B) and S3(C), respectively show the maximum signal and the signal at zero detuning

5. LASER LINEWIDTH AND TUNING RANGE

The laser linewidth can be measured experimentally, using the same heterodyne receiver that was used to recover each line frequency. In practice the linewidth stability seemed limited by the mechanical stability of the cavity. The smallest measured linewidth was recovered for one of the lowest frequency lasing lines measured (around 402.9 GHz, the $J = 8 \rightarrow 7, K = 4$ transition). The

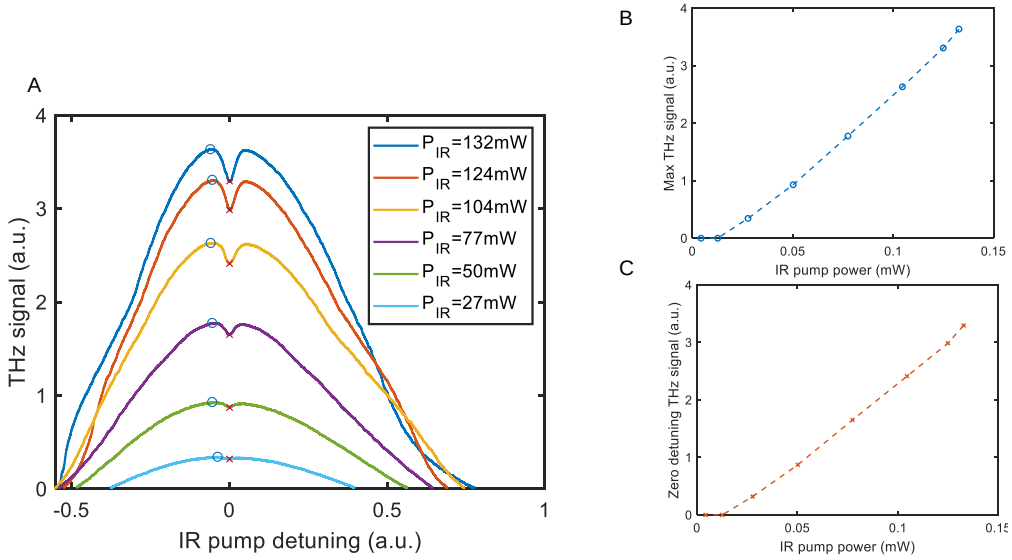

Fig. S3. (A) Plot showing the THz signal measured by the detector as a function of the pump detuning (obtained by a temperature scan of the pump QCL) for different pump powers. This corresponds to the lasing transition around 604 GHz between $J = 12 \rightarrow 11$, K=3. Plot of the THz signal as a function of the pump power for the same transition (B) for the maximum signal and (C) for zero detuning.

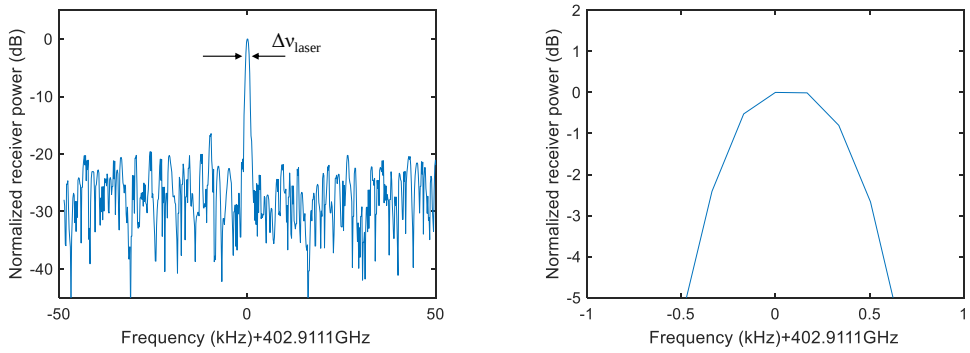

Fig. S4. Plot showing the measured line and a detail of the 3 dB linewidth for the lasing transition around 402.9 GHz, corresponding to the $J = 8 \rightarrow 7, K = 4$ molecular transition.

recovered linewidth was less than 1 kHz, and a detailed view is shown in Fig. S4.

The laser line can be tuned within the molecular gain bandwidth by a cavity pulling effect, as shown in Fig. S5. Because of the larger pressure broadening coefficient of methyl fluoride, along with a lower lasing threshold in our current laser cell compared to the previous work with N_2O, the frequency-dependent tuning range achieved by cavity pulling (around 5 MHz near 604 GHz) was approximately 10 times larger than observed with N_2O.

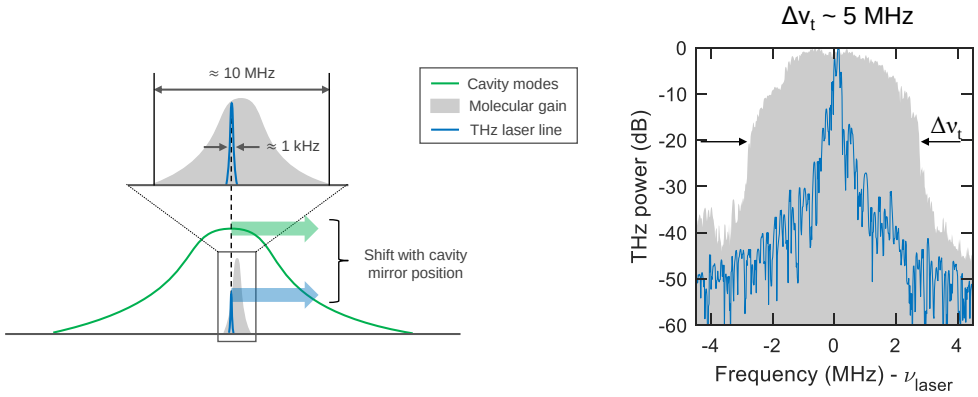

Fig. S5. (A) Schematic of the principle of cavity pulling: the cavity mode – with a larger bandwidth than the molecular gain – can be moved by tuning the cavity length. Lasing happens at the frequency with the lowest lasing threshold, that depends on the relative position of the gain bandwidth and of the cavity mode. (B) The blue curve shows a recovered frequency measured with the heterodyne mixer around 604 GHz ($J = 12 \rightarrow 11, K = 3$ transition) for a pump power of 150 mW and a gas pressure of 30 mTorr. The gray background corresponds to the envelope of all measured lasing frequencies obtained by tuning the cavity mirror by small steps.

6. OUTPUT THZ POWER AND LASING THRESHOLD

A. Simple model

The THz emission power can be estimated using a simple model [3] that assumes a very low pressure scenario with the rate of unfavorable molecular dipole-dipole collisions much smaller than the rate of favorable hard collisions with cavity walls. This model also assumes a perfect match between the QCL emission linewidth with the gain medium absorption bandwidth. In such case, the THz emission power P_{THz} at the emission frequency ν_{THz} can be estimated using the following equation [3]:

$$P_{THz} = \frac{T}{4}\frac{\nu_{THz}}{\nu_{IR}}\frac{\alpha_{IR}}{\alpha_{cell}}\left(P_{QCL} - P_{th}\right) \tag{S3}$$

where α_{IR} is the IR absorption of the gain medium at the pump frequency ν_{IR}, α_{cell} represents the total THz losses of the laser cavity, T is the output coupling fraction, P_{QCL} is the QCL pump power absorbed by the gain medium (which corresponds to the injected IR power minus the power absorbed by THz cavity walls), and P_{th} is the threshold power as expressed below:

$$P_{th} = \frac{h}{4\pi}\frac{\nu_{IR}}{\alpha_{IR}}(\alpha_{\text{cell}} R_{\text{cell}})\frac{u^2}{|\langle J_L|\mu|J_U\rangle|^2} \tag{S4}$$

where R_{cell} is the radius of the THz cavity, u is the average absolute molecular velocity, and $\langle J_L|\mu|J_U\rangle$ is the transition dipole matrix element of the lasing rotational transition.

The lasing transition dipole element can be expressed as a function of the molecular permanent dipole moment μ_0 and the J and K quantum numbers [1]:

$$|\langle J, K, V|\mu|J+1, K, V\rangle|^2 = \mu_0^2 \frac{(J+1)^2 - K^2}{(J+1)(2J+3)} \tag{S5}$$

B. Strength of the infrared transitions

In the simple model given in equation S3, the THz power is expressed as a function of the absorption coefficient $\alpha_I R$, which can be calculated as follows:

$$\alpha_{IR} = \frac{1 - \exp(-\alpha_0 L)}{L} \tag{S6}$$

where L is the cavity length, and α_0 is the IR absorption coefficient for a given roto-vibrational transition and is proportional to the square of the transition dipole matrix element [4]:

$$\alpha_0((J,K,V) \to (J',K',V')) \propto |\langle J,K,V|\mu|J',K',V'\rangle|^2 \tag{S7}$$

In the case where either the cell is short or the absorption strength is small we have $\alpha_0 L \ll 1$, which leads to $\alpha_{IR} \approx \alpha_0$. The absorption coefficient α_0 strongly depends on the population of energy levels, which is determined by the Boltzmann distribution and the molecular degeneracy.

The value of the dipole matrix element of an IR roto-vibrational transition depends on the type of the transition (P, Q, or R) and the initial and final quantum numbers [1]:

$$|\langle J+1,K,V+1|\mu|J,K,V\rangle|^2_R \propto \mu_0^2 \frac{(J+1)^2 - K^2}{(J+1)(2J+1)} \tag{S8}$$

$$|\langle J,K,V+1|\mu|J,K,V\rangle|^2_Q \propto \mu_0^2 \frac{K^2}{J(J+1)} \tag{S9}$$

From Eq. S8 and Eq. S9 one can see that Q-branch transitions($\Delta J = 0$) will be more efficient to pump large K values (i.e. K close to J), while P or R-branch transitions ($\Delta J = 1$ or -1) will be more efficient to pump small K values (i.e. K close to zero), as demonstrated in Fig .3(C) of the manuscript.

The molecular degeneracy increases proportionally to the value of J, but population decreases according to Boltzmann distribution. Degeneracy is highest at non-zero K lines multiples of 3 ($K = 3, 6$, etc.), leading to larger populations and, therefore, stronger IR absorption coefficients than neighboring lines, as can be seen in the Fig. 1(B) of the main text.

C. Normalized threshold and power efficiency

The relative IR absorption line strength used to estimate the relative QPML performance for a given J, K is estimated by the following expression:

$$L(J_{initial}, J_{final}, K) = |\langle J_{final},K,V+1|\mu|J_{initial},K,V\rangle|^2 Pop(J_{initial},K) \tag{S10}$$

The normalized power efficiency is calculated as follows for Q and R branch, respectively: the relative IR absorption line strength is multiplied by the relative lasing frequency as a function of the lower level lasing quantum number J_L and K

$$\begin{aligned} \eta_Q(J_L,K) &= (J_L)L(J_L,J_L,K) \\ &= (J_L)|\langle J_L,K,V+1|\mu|J_L,K,V\rangle|^2 Pop(J_L,K) \end{aligned} \tag{S11}$$

$$\begin{aligned} \eta_R(J_L,K) &= (J_L+1)L(J_L,J_L+1,K) \\ &= (J_L+1)|\langle J_L+1,K,V+1|\mu|J_L,K,V\rangle|^2 Pop(J_L,K) \end{aligned} \tag{S12}$$

The normalized lasing threshold is calculated for Q and R branch respectively, by taking the inverse of the line strength and the lasing matrix element as a function of the lower level lasing quantum number J_L and K

$$\begin{aligned} Th_Q(J_L,K) &= \frac{1}{|\langle J,K,V|\mu|J+1,K,V\rangle|^2 L(J_L,J_L,K)} \\ &= \frac{1}{|\langle J,K,V|\mu|J+1,K,V\rangle|^2 |\langle J_L,K,V+1|\mu|J_L,K,V\rangle|^2 Pop(J_L,K)} \end{aligned} \tag{S13}$$

$$\begin{aligned} Th_R(J_L,K) &= \frac{1}{|\langle J_L,K,V|\mu|J_L+1,K,V\rangle|^2 L(J_L,J_L+1,K)} \\ &= \frac{1}{|\langle J_L,K,V|\mu|J_L+1,K,V\rangle|^2 |\langle J_L+1,K,V+1|\mu|J_L,K,V\rangle|^2 Pop(J_L,K)} \end{aligned} \tag{S14}$$

REFERENCES

1. C. H. Townes and A. L. Schawlow, *Microwave spectroscopy* (Dover Publications, 1975).
2. D. J. Phillips, E. A. Tanner, F. C. De Lucia, and H. O. Everitt, "Infrared-terahertz double-resonance spectroscopy of ch 3 f and ch 3 cl at atmospheric pressure," Phys. Rev. A **85**, 052507 (2012).
3. P. Chevalier, A. Amirzhan, F. Wang, M. Piccardo, S. G. Johnson, F. Capasso, and H. O. Everitt, "Widely tunable compact terahertz gas lasers," Science **366**, 856–860 (2019).
4. P. W. Atkins and R. S. Friedman, *Molecular quantum mechanics* (Oxford university press, 2011).